



Nanoceria supported rhodium(0) nanoparticles as catalyst for hydrogen generation from methanolysis of ammonia borane

Derya Özhava, Saim Özkar*

Department of Chemistry, Middle East Technical University, 06800 Ankara, Turkey



ARTICLE INFO

Keywords:

Hydrogen generation
Ammonia borane
Methanolysis
Nanoceria
Rhodium(0) nanoparticles

ABSTRACT

This work reports the preparation and catalytic use of nanoceria supported rhodium(0) nanoparticles, Rh(0)/nanoCeO₂, as catalyst for hydrogen generation from the methanolysis of ammonia borane. Rh(0)/nanoCeO₂ was *in situ* formed from the reduction of rhodium(II) octanoate on the surface of nanoceria during the catalytic methanolysis of ammonia borane at room temperature. The results of analysis using PXRD, TEM, STEM-EDS, XPS, SEM, SEM-EDX, N₂ adsorption-desorption and ICP-OES reveal that rhodium(0) nanoparticles were well dispersed on the surface of nanoceria with an average size of 3.9 ± 0.6 nm. Rh(0)/nanoCeO₂ shows high catalytic activity in the methanolysis of ammonia borane with a turnover frequency of 144 min⁻¹. Note that hydrogen generation from the methanolysis of ammonia borane catalyzed by Rh(0)/nanoCeO₂ is slightly less than 3.0 equivalent, due to the reduction of Ce⁴⁺ ions to Ce³⁺ ions on the surface of nanoceria during the methanolysis of ammonia borane. The reduction of Ce⁴⁺ ions leading to the formation of Ce³⁺ defects on the surface of nanoceria under the catalytic reaction conditions could be investigated by high resolution Ce 3d XPS analysis. Additionally, the formation kinetic of rhodium(0) nanoparticles could be studied by using the hydrogen generation from the methanolysis of ammonia borane as reporter reaction; thus, the rate constants for the slow nucleation, k₁ and autocatalytic surface growth of rhodium(0) nanoparticles, k₂ were determined. Our report also includes the results of kinetic study of the catalytic methanolysis of ammonia borane depending on rhodium concentration and temperature.

1. Introduction

Ammonia borane (NH₃BH₃, AB) appears to be one of the most important hydrogen storage materials due to its high hydrogen content (19.6 wt.%), nontoxicity and high stability in solution and solid state under ambient conditions [1,2]. The use of AB as hydrogen storage material is expected to play a vital role in transition from the fossil fuels to the renewable energy sources on the way towards a sustainable energy future [3,4]. One of the efficient ways of releasing H₂ gas stored in AB is its methanolysis reaction (Eq. (1), which occurs in the presence of suitable catalysts [5,6] and might be considered as an alternative to the hydrogen evolution reaction [7].



To date, many transition metal heterogeneous catalysts have been tested in the methanolysis of AB: Cu [8–10], Cu-Pd [11], Cu-Ni [12], Ni [13], Co-Ni, [14], Co-Pd [15], Pd [16,17], Ag-Pd [18], Ru [19–21], Rh [22,23]. Among them, noble metal rhodium and ruthenium nanoparticles provide the highest catalytic activity in hydrogen generation

from the methanolysis of AB. Since the transition metal nanoparticles have tendency to agglomerate to larger particles, which causes a significant decrease in catalytic activity, they need to be stabilized against agglomeration by supporting on materials with large surface area [24–26]. In our ongoing research on the use of oxide nanopowders as supporting materials, we have recently reported the use of nanopowders of hydroxyapatite [27], silica [28], and alumina [29] to stabilize rhodium(0) nanoparticles, which were found to be highly active and long lived catalysts in hydrogen generation from the methanolysis of AB. In recent reports, one observes an increasing interest in using ceria (CeO₂) as support for the transition metal nanoparticles [30,31]. As a reducible oxide, ceria contains cerium(III) defects which can easily be formed on the surface of cerium oxides due to the high positive standard potential of Ce⁴⁺ → Ce³⁺ (1.76 V in acidic solution) [32]. The presence of cerium(III) defects causes an excess negative charge accumulation on the oxide surface. The charge balance on the oxide surface can be established by the coordination of metal(0) nanoparticles to oxide surface, which provides strong metal-support interaction, in particular, of the electron rich late transition metal nanoparticles

* Corresponding author.

E-mail address: sozkar@metu.edu.tr (S. Özkar).

[33–35]. In recent years, ceria supported metal nanoparticles have been employed as catalysts in many important reactions such as oxidation of organic compounds [36] and CO [37,38], hydrogenation of aromatics [39], decomposition of N₂O and acetic acid [40,41], hydrogen generation from hydrolysis of AB [42–45], dehydrogenation of formic acid [46], ethanol steam reforming [47]. The formation of small clusters (such as Pt, Rh or Pd) on the surface of ceria has been widely elucidated in the literature. Nehasil and co-workers demonstrated, using a set of spectroscopic methods and DFT calculations, that there is a fast charge transfer from rhodium to ceria [48]. This charge transfer induces the formation of Rh⁺^δ and Ce³⁺ states that may enhance the catalytic activity [49].

Herein we report the use of nanoceria with an average particle size of 25 nm as support for stabilizing rhodium(0) nanoparticles. Nanoceria supported rhodium(0) nanoparticles, hereafter referred to as (Rh(0)/nanoCeO₂), were *in situ* formed from reduction of rhodium(II) ions impregnated on nanoceria during the methanolysis of AB in methanol. After isolation from reaction solution, Rh(0)/nanoCeO₂ was characterized using a combination of advanced analytical methods including PXRD, TEM, STEM-EDS, XPS, SEM, SEM-EDX, N₂ adsorption desorption and ICP-OES. The results of XPS investigation particularly support the claim of increasing concentration of Ce³⁺ defects during the catalytic reaction. Our report also includes the comparison of Rh(0)/nanoCeO₂ with the rhodium(0) nanoparticles supported on other oxide nanopowders of alumina, silica and hydroxyapatite in terms of catalytic activity as well as kinetics of catalytic methanolysis of AB.

2. Experimental

2.1. Materials

Rhodium(II) octanoate, ammonia borane (97%), methanol (99%), and nanoceria (CeO₂, particle size ≈ 25 nm) were purchased from Aldrich. Methanol was distilled over Mg metal and kept under nitrogen atmosphere until its use in methanolysis.

2.2. Instrumentation

The samples used for STEM-EDS, XPS, PXRD, SEM or N₂ adsorption desorption analysis were harvested from *in situ* generated Rh(0)/nanoCeO₂ solution at the end of catalytic methanolysis of AB. After the settling the powders, supernatant solution was taken out using a capillary syringe. The remaining powder was dried in vacuum at room temperature. The X-ray photoelectron spectroscopy (XPS) analysis was performed on a Physical 15 Electronics 5800 spectrometer equipped with a hemispherical analyzer and using monochromatic Al K α radiation of 1486.6 eV, the X-ray tube working at 15 kV, 350 W and pass energy of 23.5 keV. The X-ray diffraction (XRD) pattern was recorded on a MAC Science MXP 3TZ diffractometer using Cu-K α radiation (wavelength 1.5406 Å, 40 kV, 55 mA). The nitrogen adsorption/desorption experiments were carried out at 77 K using a NOVA 3000 series Quantachrome Instrument. The sample was out gassed under vacuum at 573 K for 3 h before the adsorption of nitrogen. SEM analyses were run on a JEOL JSM-5310LV operating at 15 kV and 33 Pa in a low-vacuum mode without metal coating on the aluminium support. The TEM samples were harvested from *in situ* generated Rh(0)/nanoCeO₂ solution at the end of catalytic methanolysis of AB. A few drops of nanoparticle solution was redispersed in 2 mL methanol and ultrasonicated for 3 min then, one drop of this solution was placed on the carbon coated copper grid of TEM and dried under inert atmosphere. Samples were examined at magnification between 100 and 400 K. STEM-EDS mapping images were recorded on a Hitachi HT7700 TEM instrument equipped with STEM and EDAX modules operated at 120 kV.

2.3. *In situ* preparation of Rh(0)/nanoCeO₂ and catalytic methanolysis of AB

Certain aliquot of a stock solution of 4.9 mM rhodium(II) octanoate is transferred into the reaction flask containing nanoceria powder, thermostated at a specified temperature by circulating water through its jacket. After addition of required amount of methanol to make the volume 7 mL, the resulting suspension is stirred for 1 h. Then, a 3.0 mL methanol solution of AB (64 mg, 2.0 mmol) is added to the flask *via* a gas tight syringe and the reaction is immediately launched. The volume of H₂ gas released is recorded by measuring the displacement of water level in the glass tube connected to the reaction flask, following the procedure described elsewhere [28]. Note that all the experiments in this study are performed under stirring at 1000 rpm to ensure that the methanolysis in the presence of Rh(0)/nanoCeO₂ catalyst is in the kinetic regime, not under mass transfer limitation.

2.4. Effect of temperature and rhodium concentration on k_1 and k_2 values

Methanolysis reaction is performed starting with a constant AB concentration (200 mM, 64 mg AB) and 50.0 mg Rh(II)/nanoCeO₂ precatalyst in different rhodium loading (1.0, 2.0 and 3.0 wt. %) and at different temperatures in the range 20–35 °C, following the procedure given in the previous section.

2.5. Catalytic lifetime of Rh(0)/nanoCeO₂ catalyst in the methanolysis of AB

A catalytic lifetime experiment of Rh(0)/nanoCeO₂ in hydrogen generation from the methanolysis of AB is performed starting with 10 mL suspension of 50 mg Rh(II)/nanoCeO₂ (1.0 wt.% rhodium, 4.9 μmol Rh) and 200 mM (64 mg) AB at 25.0 ± 0.5 °C following the procedure described elsewhere [28].

2.6. Leaching test for Rh(0)/nanoCeO₂

After the first run of catalytic methanolysis of 200 mM AB catalyzed by Rh(0)/nanoCeO₂ (1.0 wt. % Rh, 0.49 mM Rh) the reaction is stopped and opened under nitrogen inert gas atmosphere; when the nanoparticles are settled down, the supernatant solution is transferred *via* a

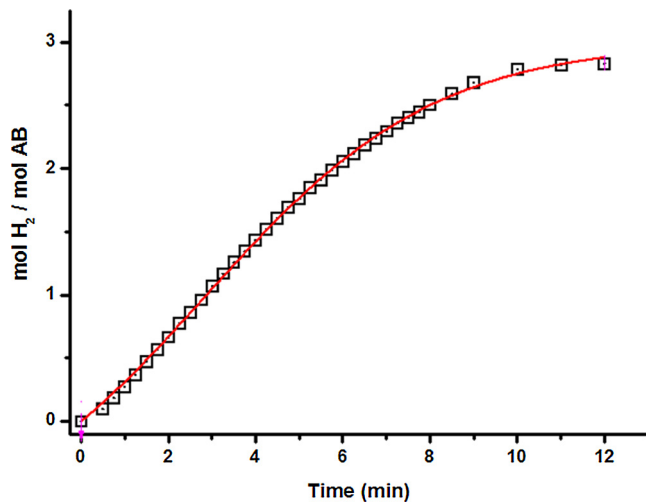
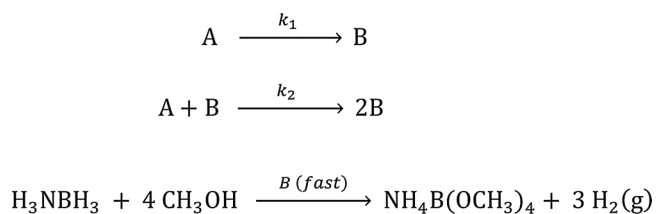


Fig. 1. Plots of mol H₂ evolved per mole of AB *versus* time for the catalytic methanolysis of AB starting with 200 mM AB and 50 mg of Rh(II)/nanoCeO₂ (1.0 wt.% Rh, [Rh] = 0.49 mM) in 10 mL methanol at 25.0 ± 0.5 °C. The red curve shows the fit of data to the FW 2-step mechanism of nanoparticle formation (For interpretation of the references to colour in this figure legend, the reader is referred to the web version of this article).



Scheme 1. Illustration of hydrogen generation from the catalytic methanolysis of AB as reporter reaction: A is the precursor Rh(II)/nanoCeO₂ and B is the growing Rh(0)_n nanoparticles on the surface of nanoceria support.

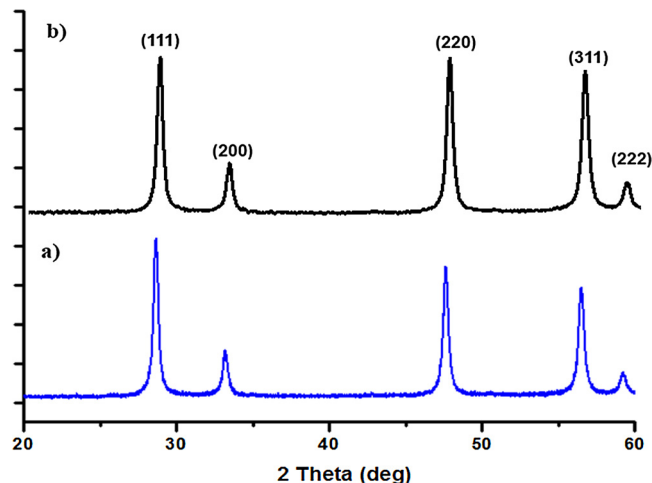


Fig. 2. Powder X-Ray diffraction patterns of a) bare nanoCeO₂ b) Rh(0)/nanoCeO₂ with rhodium loading of 1.0 wt. % Rh.

gas tight syringe into another reaction flask, and 64.0 mg AB (200 mM AB) is added. The progress of the reaction is followed by applying the procedure given elsewhere [28]. At the end of the leaching test, filtrate solution is analyzed by ICP-OES to detect any rhodium leached from the nanoceria surface to the solution during methanolysis reaction.

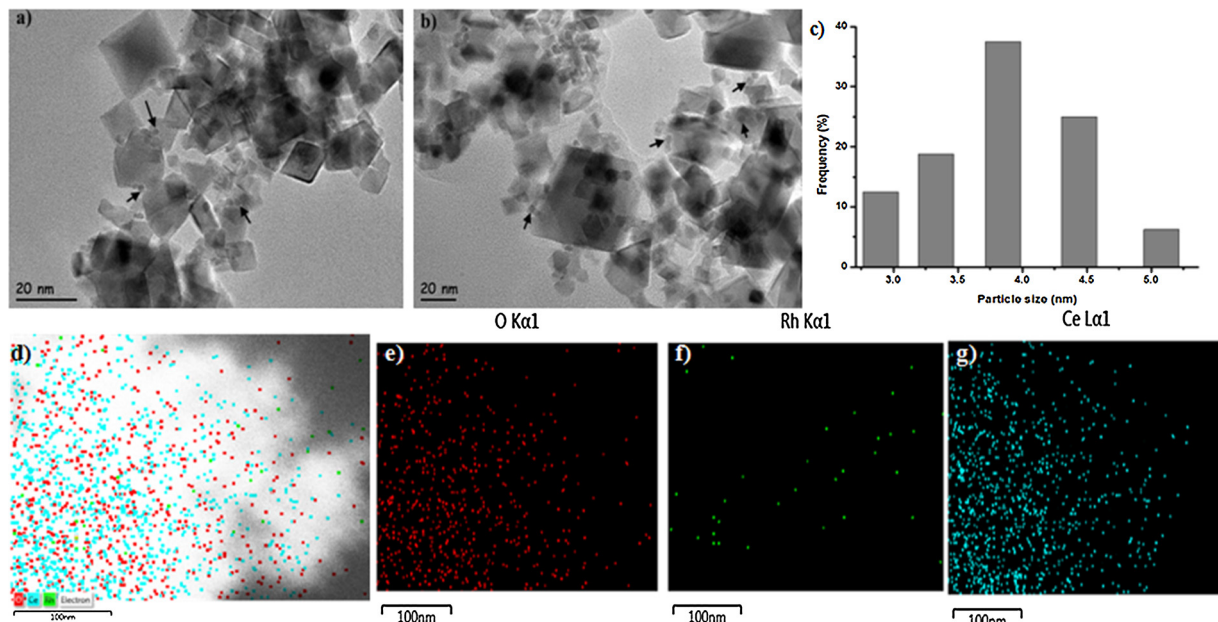


Fig. 3. (a–b) TEM images of Rh(0)/nanoCeO₂ with a rhodium loading of 1.0 wt. % Rh after catalytic methanolysis of 200 mM AB at 25.0 ± 0.5 °C. c) The corresponding histogram of rhodium(0) nanoparticle size distribution. d) STEM-EDS mapping of e) O f) Rh g) Ce.

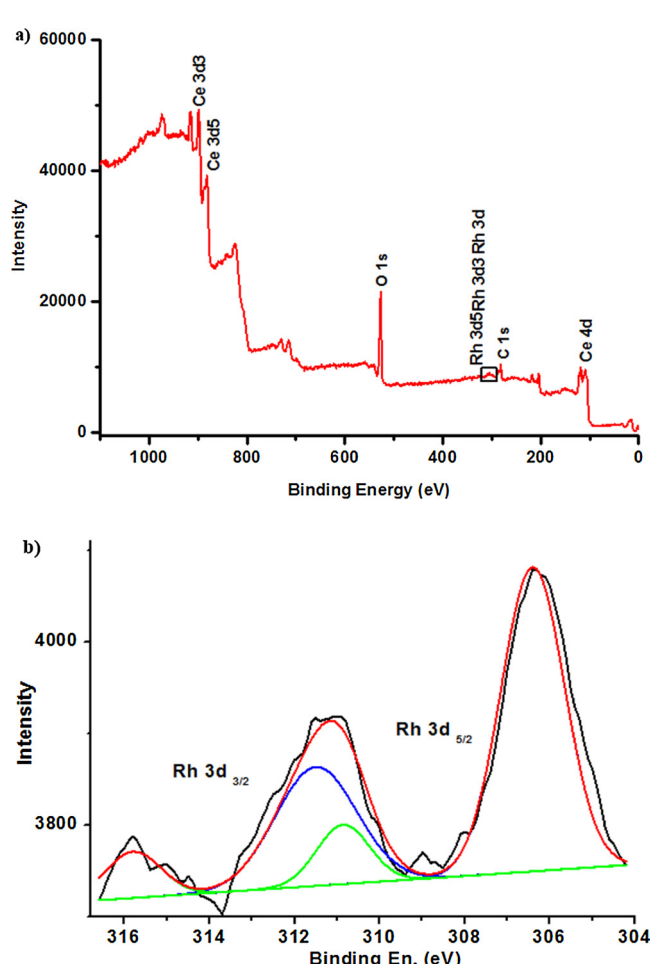


Fig. 4. a) X-ray photoelectron (XPS) survey scan spectrum, b) high resolution Rh 3d XPS spectrum of Rh(0)/nanoCeO₂ with a rhodium loading of 1.0 wt. % Rh.

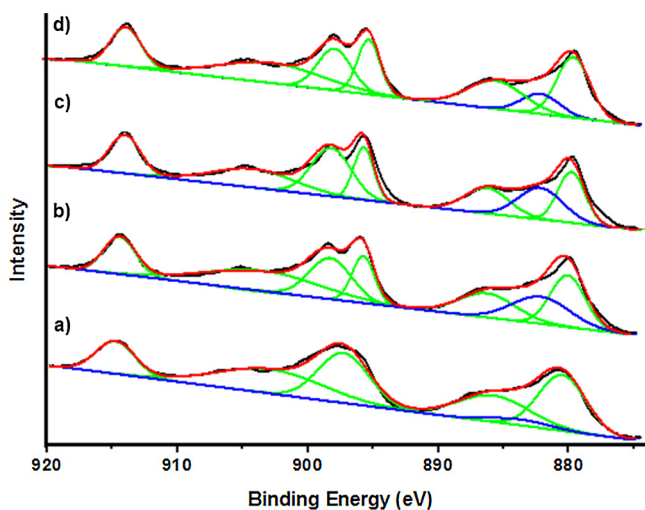


Fig. 5. High resolution Ce 3d XPS spectrum of a) bare nanoceria, b) nanoceria treated with AB in methanol, and Rh(0)/nanoCeO₂ with a rhodium loading of c) 1.0 wt. % Rh, and d) 4.0 wt. % Rh.

3. Results and discussion

Nanoceria supported rhodium(0) nanoparticles, Rh(0)/nanoCeO₂, were *in situ* formed from the reduction of rhodium(II) ions impregnated on nanoceria during the methanolysis of AB. When AB solution is added to a suspension of Rh(II)/nanoCeO₂ in methanol, both reduction of rhodium(II) ions to rhodium(0) and H₂ gas evolution from the

methanolysis of AB occur concomitantly. The progress of rhodium(0) nanoparticle formation and methanolysis of AB could be followed by monitoring the volume of H₂ gas, which was then converted into the equivalent H₂ per mole of AB, using the known 3:1 H₂/AB stoichiometry. Fig. 1 depicts the graph of mol H₂ evolved per mole of AB versus time for the methanolysis of 200 mM AB catalyzed by 0.49 mM Rh (50 mg of Rh(II)/nanoCeO₂, 1.0 wt. % Rh) in 10 mL methanol at 25.0 ± 0.5 °C. H₂ evolution starts after a short induction time less than 1 min and proceeds almost linearly until the complete consumption of AB in the reaction flask. Note that the amount H₂ gas collected is slightly less than 3.0 equivalent per mole of AB because some amount of AB is consumed to reduce Ce⁴⁺ ions to Ce³⁺ on the surface of ceria (see the results of XPS). Then, the remaining AB undergoes the methanolysis to release H₂ gas in the presence of Rh(0)/nanoCeO₂. The initial pale blue color of reaction solution turned to black during the induction period. The color change and the sigmoidal shape of hydrogen generation curve indicate that the formation of rhodium(0) nanoparticles follows the Finke-Watzky (FW) 2-step mechanism of slow, continuous nucleation (A → B, rate constant k₁) and then, autocatalytic surface growth (A + B → 2B, rate constant k₂) given in Scheme 1 [50,51], where A stands for the rhodium(II) precursor and B stands for the rhodium(0) nanoparticles.

Eq. (2) gives the integrated form of the rate law derived from FW 2-step mechanism, where [AB]_t and [AB]₀ are the concentration of AB at time t and 0, respectively [50].

$$[\text{AB}]_t = \frac{\frac{k_1}{k_2} + [\text{AB}]_0}{1 + \frac{k_1}{k_2[\text{AB}]_0} \exp(k_1 + k_2[\text{AB}]_0)t} \quad (2)$$

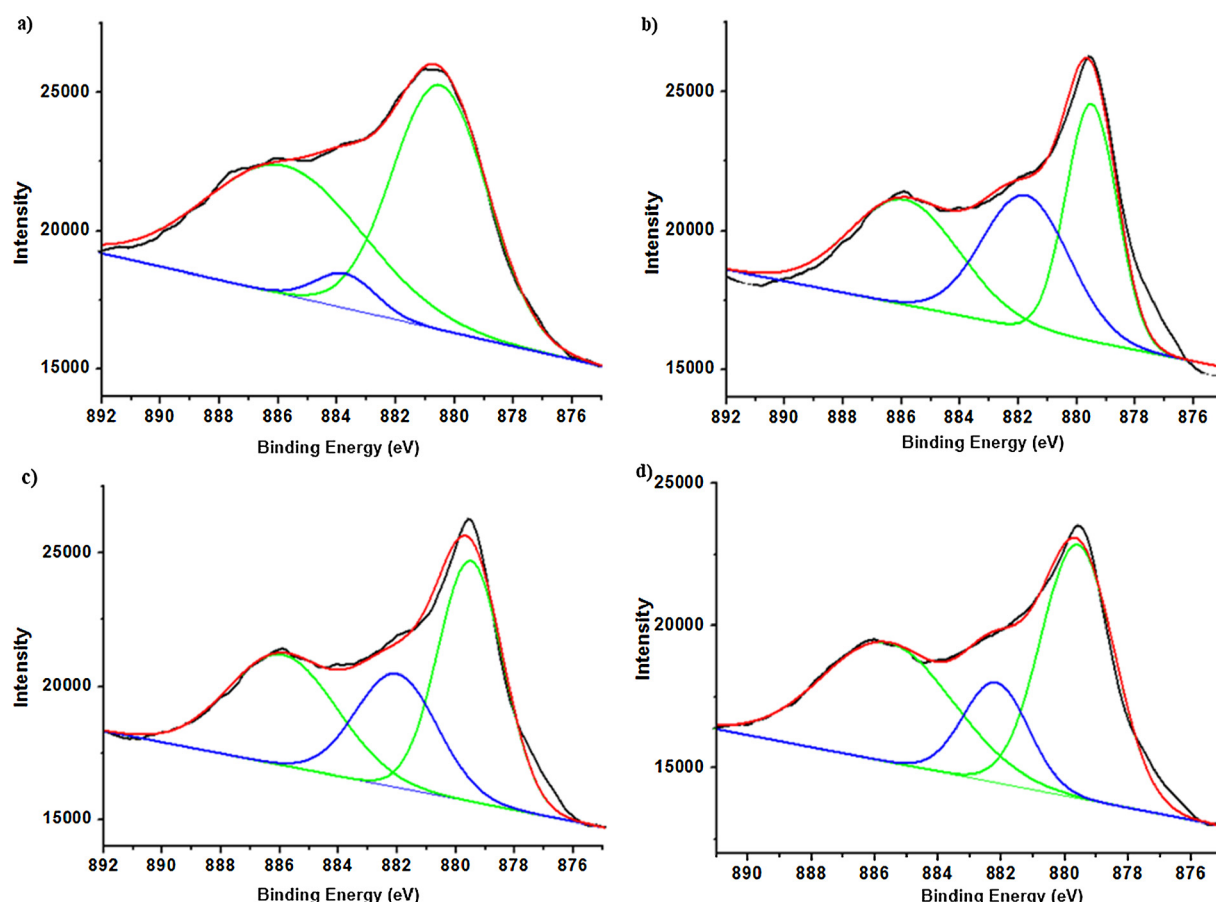


Fig. 6. High resolution Ce 3d XPS spectrum in a specified region between 890.0 and 875.0 eV for a) bare nanoceria, b) nanoceria treated with AB in methanol, and Rh(0)/nanoCeO₂ with a rhodium loading of c) 1.0 wt. % Rh, and d) 4.0 wt. % Rh.

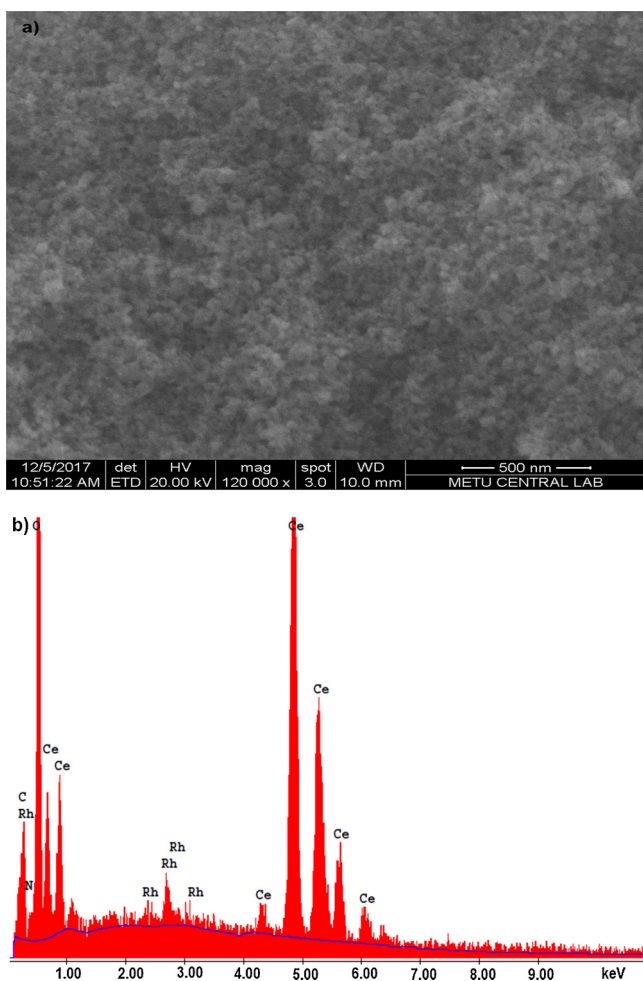


Fig. 7. a) SEM image of Rh(0)/nanoCeO₂, b) SEM-EDX spectrum of Rh(0)/nanoCeO₂ with a rhodium loading of 1.0 wt. % Rh.

Eq. (2) can be used to fit the experimental data in Fig. 1 to the FW 2-step mechanism yielding the rate constants $k_1 = 9.6 \times 10^{-2} \text{ min}^{-1}$ and $k_2 = 3.8 \times 10^1 \text{ M}^{-1} \text{ min}^{-1}$ for slow, continuous nucleation and auto-catalytic surface growth of rhodium(0) nanoparticles, respectively. The large value of k_2/k_1 ratio = 5.6×10^2 implies on the high level of kinetic control of the nanoparticles formation [50].

3.1. Characterization of Rh(0)/nanoCeO₂

Rh(0)/nanoCeO₂ could be isolated from the solution and characterized by a combination of advanced analytical methods. Fig. 2 depicts the XRD patterns of bare nanoceria and Rh(0)/nanoCeO₂. Both samples give the same XRD pattern showing the characteristic diffraction peaks of ceria at 28.5, 33.1, 47.5, 56.3 and 59.1 attributed to the (111), (200), (220), (311) and (222) reflections of ceria, respectively (JCDP Card 34-0394). Thus, it can be concluded that ceria preserves both crystallinity and the lattice after the impregnation of Rh(II) ions and their reduction to Rh(0) on nanoceria. It is noteworthy that no diffraction peaks are observable for rhodium(0) nanoparticles due to the low Rh concentration of Rh(0)/nanoCeO₂ sample.

Fig. 3 shows TEM images and STEM-EDS mapping of Rh(0)/nanoCeO₂ sample with a rhodium loading of 1.0 wt. % Rh after the catalytic methanolysis of AB. STEM-EDS mapping (Fig. 3d) reveals the uniform dispersion of rhodium(0) nanoparticles on the surface of nanoceria. The particle size of rhodium(0) nanoparticles can be determined from the TEM images in Fig. 3a-b to be in the range 2.9–5.2 nm with an average size of $3.9 \pm 0.6 \text{ nm}$ as shown in the

histogram (Fig. 3c).

Fig. 4a displays a survey scan XPS of Rh(0)/nanoCeO₂ sample with a rhodium loading of 1.0%wt. Rh indicating the existence of rhodium in addition to the framework elements of ceria (Ce and O) in agreement with the SEM-EDX results (see later). The high resolution Rh 3d XPS scan of the same sample (Fig. 4b) shows two prominent peaks at 306.4 and 311.5 eV, readily assigned to the Rh(0) 3d_{5/2} and 3d_{3/2}, respectively, by comparing to the values of metallic rhodium [52,53]. Moreover, the higher energy peaks observed at 310.9 and 315.8 eV can be ascribed to the Rh³⁺ 3d_{5/2} and 3d_{3/2}, respectively, likely in the form of oxide, which may originate from surface oxidation of rhodium(0) nanoparticles when exposed to air shortly during the XPS sampling [54,55]. Additionally, Fig. 5 shows the high resolution Ce 3d XPS scan of various nanoceria samples which allows to investigate the surface composition of ceria in terms of relative concentration of Ce³⁺ and Ce⁴⁺ ions. Cerium(III) defects can easily be formed on the surface of cerium oxides due to the high positive standard potential of Ce⁴⁺ → Ce³⁺ (1.76 eV in acidic solution) [32]. The catalytic reaction conditions can promote the interconversion of two oxidation states of cerium [56]. The high resolution Ce 3d XPS spectra in Fig. 5 exhibit two prominent peaks at 885.0 and 879.0 eV for cerium(IV) ions and a characteristic peak at 883.0 eV assigned to cerium(III) ions for all the ceria samples. The relative intensity of Ce³⁺ peak increases on passing from bare cerium oxide to the ceria treated with AB in methanol for 10 min or Rh(0)/nanoCeO₂ samples with different rhodium loading. Fig. 6 depicts the high resolution Ce 3d XPS spectra in the specified region between 890.0 and 875.0 eV, clearly presenting the changes in relative intensity of cerium(III) peak for all the ceria samples. This observation indicates that the concentration of Ce³⁺ ions on the ceria surface increases during the methanolysis reaction; that is, under catalytic conditions. The increase in Ce³⁺ concentration explains the consumption of AB for the reduction of Ce⁴⁺ to Ce³⁺ during the catalytic reaction. Therefore, the amount of H₂ gas collected during the catalytic methanolysis is slightly less than 3.0 equivalent H₂ per mole of AB (*vide infra*). It is noteworthy that the relative intensity of Ce³⁺ peak at 883.0 eV decreases as the rhodium loading is increased from 1.0 to 4.0 wt. % Rh (Fig. 6c and d). This may be due to the partial coverage of surface defects by the increasing rhodium(0) nanoparticles on the surface of nanoceria.

Fig. 7a gives the SEM image of Rh(0)/nanoCeO₂ with a rhodium loading of 1.0 wt. % Rh, which shows no bulk rhodium metal formation in noticeable size on the surface of nanoceria. SEM-EDX spectrum in Fig. 7b confirms the presence of rhodium in addition to the framework elements of ceria (Ce, O).

N₂-adsorption-desorption analysis was performed for both nanoceria and Rh(0)/nanoCeO₂ with a rhodium loading of 1.0 wt.% Rh and surface areas were found to be 48.1 and 37.0 m² g⁻¹, respectively. The slight decrease in the surface area of nanoceria can be interpreted as supplementary evidence for the existence rhodium(0) nanoparticles on the surface of nanoceria [42].

3.2. Catalytic activity of Rh(0)/nanoCeO₂ in the methanolysis of AB

As shown in Fig. 1 Rh(0)/nanoCeO₂ catalysts have excellent performance in hydrogen generation from the methanolysis of AB even in low rhodium concentration at 25.0 ± 0.5 °C. Fig. 8 shows the plots of mol H₂ evolved per mole of AB versus time during the catalytic methanolysis of 200 mM AB starting with Rh(II)/nanoCeO₂ precursor of different rhodium loading (1.0, 2.0, 3.0 and 4.0 wt. % Rh), thus in different rhodium concentrations, at 25.0 ± 0.5 °C. In all cases, hydrogen evolution starts after a short induction period and continues almost linearly until the complete consumption of AB present in the solution. Note that the linear portions of plots present the constant hydrogen generation rate which indicates the structure insensitivity of methanolysis of AB catalyzed by Rh(0)/nanoCeO₂ as well as the presence of a zero order reaction with respect to the concentration of AB

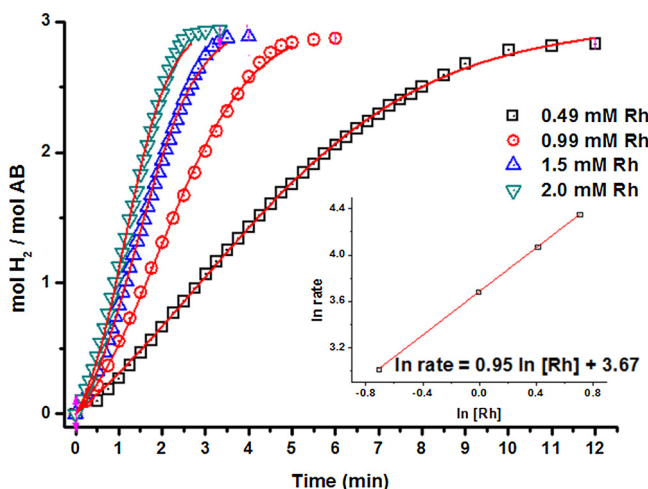


Fig. 8. Plots of mol H_2 evolved per mole of AB versus time for methanolysis of 200 mM AB in different metal concentrations ($[\text{Rh}] = 0.49, 0.99, 1.5$ and 2.0 mM , each prepared using metal loading of 1.0, 2.0, 3.0, 4.0 wt.% Rh, respectively) at $25.0 \pm 0.5^\circ\text{C}$. Inset: Plot of hydrogen generation rate versus the concentration of rhodium (both in logarithmic scale).

substrate. Kinetic data in Fig. 8 fit well to FW 2-step mechanism yielding the rate constants k_1 and k_2 for the nucleation and autocatalytic growth of nanoparticle formation [50], which are listed in Table 1 together with the rate of hydrogen generation and turnover frequency values calculated from the plots in Fig. 8. The comparison of initial TOF values shows that Rh(0)/nanoCeO₂ with rhodium concentration of 0.49 mM Rh (1.0 wt. % Rh) exhibits the highest catalytic activity with an initial TOF value of 144 min^{-1} (496 min^{-1} corrected for surface Rh atoms). Plotting the hydrogen generation rate versus the initial rhodium concentration, both in logarithmic scale, gives straight line with a slope of $0.95 \approx 1.0$ (The inset of Fig. 8) indicating that the methanolysis of AB catalyzed by Rh(0)/nanoCeO₂ is first order with respect to rhodium concentration.

Fig. 9 shows the plots of mol H_2 evolved per mole of AB versus time for the methanolysis of AB starting with 200 mM AB plus 50.0 mg Rh(II)/nanoCeO₂ precatalyst in different rhodium loading (1.0, 2.0 and 3.0 wt. % Rh) at different temperatures (20, 25, 30 and 35 °C). The rate constants k_1 for the slow, continuous nucleation and k_2 for the autocatalytic surface growth could be obtained by fitting the kinetic data to the FW 2-step mechanism Eq. (2) and listed in Table 2. From the temperature dependent rate constants one can calculate the activation energies for the individual nucleation and autocatalytic surface growth steps of rhodium(0) nanoparticle formation for each rhodium concentration by using the Arrhenius equation. The resulting activation energy values are also listed in Table 2. Inspection of the data listed in Table 2 ascertains the following points: (i) the rate constant k_1 value increases with increasing temperature for each rhodium loading and, parallel to this, the induction period decreases with increasing temperature as the induction period has been shown to be inversely proportional to the nucleation rate constant [50]. (ii) Similarly, the rate

constant k_2 value increases with the increasing temperature for each rhodium loading. (iii) One observes a general trend of increasing k_1 and k_2 values with the increasing rhodium loading at each temperature. (iv) While a general trend of decreasing activation energy for the autocatalytic surface growth step is noted as the rhodium loading increases, no trend is noticeable in the activation energy for the nucleation step of nanoparticle formation.

Activation parameters for the methanolysis of AB catalyzed by Rh(0)/nanoCeO₂ can be determined from the temperature dependent kinetic data displayed in Fig. 9 for each rhodium concentration. The reaction rate constant k_{obs} of the methanolysis can be obtained from the slope of the linear part of each hydrogen generation versus time plot at different temperatures. Activation energy obtained using Arrhenius equation is 75.0 ± 2.0 , 71.9 ± 2.0 and $64.6 \pm 2.0 \text{ kJ.mol}^{-1}$ for the catalytic methanolysis reaction catalyzed by Rh(0)/nanoCeO₂ with the rhodium loading of 1.0, 2.0 and 3.0 wt. % Rh, respectively. The increase in rhodium concentration causes a noticeable decrease in the activation energy for the catalytic methanolysis of AB.

Total turnover number (TTN) of Rh(0)/nanoCeO₂ in the methanolysis of AB was determined in a catalytic lifetime experiment starting with 10 mL suspension of Rh(II)/nanoCeO₂ containing 0.49 mM Rh and 200 mM AB at $25.0 \pm 0.5^\circ\text{C}$ (Fig. 10). When hydrogen generation tends to stop, a new batch of AB was added into reaction flask. This procedure was continued until no more H_2 gas evolution was observed. Rh(0)/nanoCeO₂ provided a minimum of 5400 turnovers over 24 h before deactivation with an initial turnover frequency (TOF) value of 144 min^{-1} in hydrogen generation from the methanolysis of AB at $25.0 \pm 0.5^\circ\text{C}$. As anticipated, the TOF value decreases in the course of lifetime experiment because of the increasing viscosity due the continuous addition of AB or deactivating effect of boron containing by products. Rh(0)/nanoCeO₂ provides a lower initial turnover frequency (TOF = 144 min^{-1}) compared to our previously reported rhodium catalysts in the same reaction: Rh(0)/nanoHAP (TOF = 147 min^{-1}) [27], Rh(0)/nanoSiO₂ (TOF = 168 min^{-1}) [28] or Rh(0)/nanoAl₂O₃ (TOF = 218 min^{-1}) [29]. However, this value is still higher than TOFs of the other catalysts reported in literature for the same reaction: RhCl₃ (TOF = 100 min^{-1}) [5], zeolite confined rhodium(0) nanoparticles (TOF = 30 min^{-1}) [22], MMT-immobilized ruthenium(0) nanoparticles (TOF = 90.9 min^{-1}) [20], graphene supported ruthenium(0) nanoparticles (TOF = 99.4 min^{-1}) [21].

3.3. Leaching test for Rh(0)/nanoCeO₂ in the methanolysis of AB

An important issue in working with the supported nanoparticle catalysts is to check whether the nanoparticles are chemically transferred from the support surface to the solution during the catalytic reaction, where they may continue to contribute to the catalysis. In the present study, the hydrogen generation from the methanolysis of AB is expected to be stopped by the removal of Rh(0)/nanoCeO₂ catalyst from the reaction medium if there is no leaching of rhodium from the ceria surface to the solution. Such a control experiment was performed starting with 200 mM AB plus 50 mg Rh(II)/nanoCeO₂ (1.0 wt. % Rh, $[\text{Rh}] = 0.49 \text{ mM}$) in 10 mL methanol at $25.0 \pm 0.5^\circ\text{C}$. After the complete methanolysis of AB, solid Rh(0)/nanoCeO₂ was allowed to settle down then, supernatant solution was transferred via a gas tight syringe

Table 1

The rate constants k_1 of the slow, continuous nucleation, A → B, and k_2 of the autocatalytic surface growth, A + B → 2B, for the formation of rhodium(0) nanoparticles catalyst from the reduction of rhodium(II) ions during the methanolysis of AB (200 mM) starting with Rh(II)/nanoCeO₂ having different rhodium loading, rhodium concentrations, hydrogen generation rates, turnover frequency (TOF) values at $25.0 \pm 0.5^\circ\text{C}$.

wt.%Rh	[Rh] (mM)	$k_1 (\text{min}^{-1})$	$k_2 (\text{M}^{-1} \text{min}^{-1})$	k_2 / k_1	H_2 generation rate ($\text{mmol} \cdot \text{min}^{-1}$)	TOF (min^{-1})
1.0	0.49	$(9.58 \pm 0.14) \times 10^{-2}$	39.0 ± 0.8	407	0.75	144
2.0	0.99	$(12.9 \pm 0.54) \times 10^{-2}$	56.3 ± 1.9	436	1.47	134
3.0	1.5	$(16.6 \pm 0.44) \times 10^{-2}$	57.9 ± 1.1	349	2.18	128
4.0	2.0	$(18.8 \pm 0.76) \times 10^{-2}$	59.9 ± 1.6	317	2.76	122

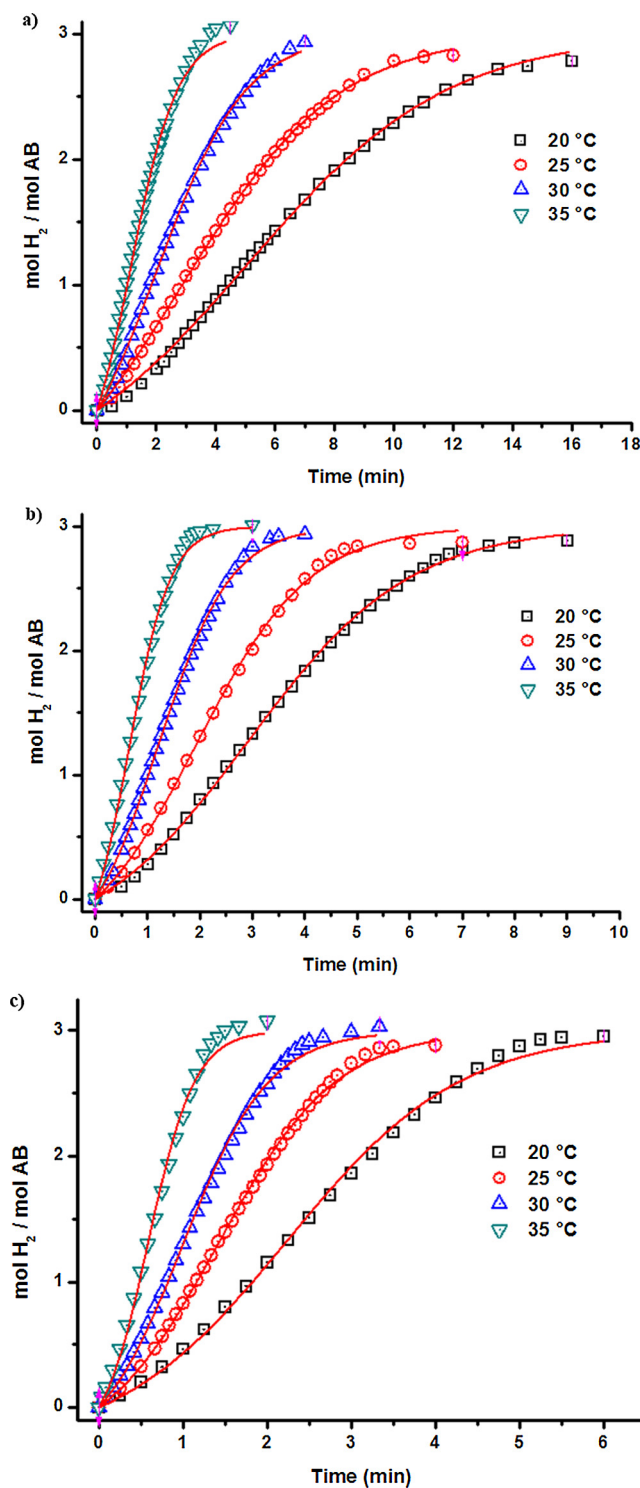


Fig. 9. Plots of mol H_2 evolved per mole of AB versus time for the catalytic methanolysis of AB at various temperatures in the range of 20–35 °C keeping the concentration of substrate at $[\text{AB}] = 200 \text{ mM}$ and varying the concentration of rhodium a) 1.0 wt. % Rh, $[\text{Rh}] = 0.49 \text{ mM}$, b) 2.0 wt. % Rh, $[\text{Rh}] = 0.99 \text{ mM}$, c) 3.0 wt. % Rh, $[\text{Rh}] = 1.5 \text{ mM}$, respectively.

into another reaction flask under inert gas atmosphere. A new batch of solid AB was added to supernatant solution and the solution was stirred for an hour at $25.0 \pm 0.5^\circ\text{C}$. During that period, no hydrogen gas evolution was observed indicating that rhodium(0) nanoparticles are well stabilized on the surface of nanoceria; thus no rhodium leaches from the surface of nanoceria into the reaction solution during

Table 2
The rate constants k_1 of the slow, continuous nucleation, $\text{A} \rightarrow \text{B}$, and k_2 of the autocatalytic surface growth, $\text{A} + \text{B} \rightarrow 2\text{B}$, for the formation of rhodium(0) nanoparticles catalyst from the reduction of rhodium(II) ions during the methanolysis of AB, k_{obs} values for the catalytic methanolysis reaction, activation energies for the nucleation and autocatalytic surface growth steps as well as the methanolysis of AB catalyzed by Rh(0)/ CeO_2 having different rhodium concentrations.

[Rh]	0.49 mM			0.99 mM			1.5 mM		
	$k_1 (\text{min}^{-1})$	$k_2 (\text{M}^{-1} \text{min}^{-1})$	$k_{\text{obs}} (\text{molH}_2 \text{ molRh}^{-1} \text{ s}^{-1})$	k_1	k_2	$k_{\text{obs}} (\text{molH}_2 \text{ molRh}^{-1} \text{ s}^{-1})$	k_1	k_2	$k_{\text{obs}} (\text{molH}_2 \text{ molRh}^{-1} \text{ s}^{-1})$
293	$5.41 \times 10^{-2} \pm 1.11 \times 10^{-3}$	32.6 ± 0.8	1.50	$8.40 \times 10^{-2} \pm 1.99 \times 10^{-3}$	38.2 ± 0.7	1.49	$9.95 \times 10^{-2} \pm 5.41 \times 10^{-3}$	39.3 ± 1.4	1.28
298	$9.60 \times 10^{-2} \pm 1.44 \times 10^{-3}$	38.5 ± 0.8	2.24	$1.31 \times 10^{-1} \pm 5.36 \times 10^{-3}$	53.8 ± 1.8	2.05	$1.67 \times 10^{-1} \pm 4.22 \times 10^{-3}$	57.1 ± 1.1	1.98
303	$1.38 \times 10^{-1} \pm 3.40 \times 10^{-3}$	71.9 ± 2.0	3.78	$2.13 \times 10^{-1} \pm 5.03 \times 10^{-3}$	83.7 ± 1.7	3.35	$2.46 \times 10^{-1} \pm 9.87 \times 10^{-3}$	77.2 ± 2.4	2.82
308	$2.41 \times 10^{-1} \pm 9.11 \times 10^{-3}$	139.1 ± 5.6	6.69	$4.15 \times 10^{-1} \pm 1.98 \times 10^{-2}$	142.7 ± 6.1	6.26	$3.83 \times 10^{-1} \pm 3.34 \times 10^{-2}$	146 ± 8.9	4.95
Activation En. (kJ/mol)	73.5	74.4	75.0	79.1	65.9	71.9	66.5	63.5	64.6

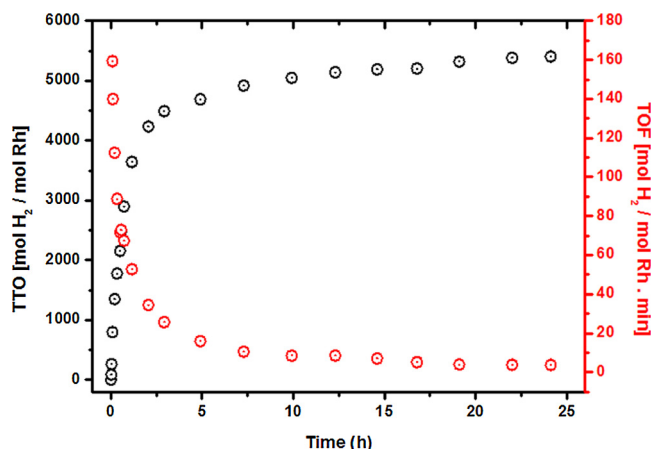


Fig. 10. Plot of total turnover number (TTO) or turnover frequency *versus* time for the methanolysis of AB with 10 mL solution of 0.49 mM Rh (50.0 mg Rh(0)/nanoCeO₂, 1.0 wt.% Rh,) and 200 mM AB (for each run) at 25.0 ± 0.5 °C.

methanolysis. The supernatant solution was also examined by ICP-OES analysis to detect rhodium present in the solution; the rhodium concentration in supernatant solution is found to be 0.008 mM which is negligible compared to the initial rhodium concentration of 0.491 mM in the reaction solution. Therefore, it can be concluded that Rh(0)/nanoCeO₂ are kinetically competent and heterogeneous catalyst in the methanolysis of AB.

4. Conclusions

Nanoceria supported rhodium(0) nanoparticles (Rh(0)/nanoCeO₂) were *in situ* prepared with an easy and reproducible method, then isolated and characterized with advance analytical techniques. The formation kinetics of rhodium(0) nanoparticles could be studied by fitting the H₂ evolution *versus* time plots to the FW 2-step mechanism providing the rate constants k_1 of the slow, continuous nucleation and k_2 of the autocatalytic surface growth for the formation of rhodium(0) nanoparticles from reduction of rhodium(II) precursor during the methanolysis. Rh(0)/nanoCeO₂ catalysts have excellent performance in hydrogen generation from the methanolysis of AB even in low rhodium concentration at 25.0 ± 0.5 °C. It is noteworthy that methanolysis of AB catalyzed by Rh(0)/nanoCeO₂ provides slightly less than 3.0 equivalents H₂ per mole of AB because of the consumption of AB for the reduction of Ce⁴⁺ to Ce³⁺ during the catalytic reaction. The formation of Ce³⁺ defects could be confirmed by XPS analysis which shows the increase in Ce³⁺ concentration on the surface of nanoceria on passing from bare cerium oxide to the ceria treated with AB in methanol for 10 min or Rh(0)/nanoCeO₂ samples with different rhodium loading. Rhodium(0) nanoparticles have uniform dispersion on the surface of nanoceria with an average particle size of 3.9 ± 0.6 nm. Rh(0)/nanoCeO₂ provides a minimum of 5400 turnovers over 24 h before deactivation with an initial turnover frequency (TOF) value of 144 min⁻¹ in hydrogen generation from methanolysis of AB 25.0 ± 0.5 °C. The effect of temperature and rhodium concentration on k_1 and k_2 values, thus the variation of activation energies for the individual nucleation and autocatalytic surface growth steps of rhodium(0) nanoparticle formation in the methanolysis of AB could be examined by performing a series experiments with Rh(0)/nanoCeO₂ in different rhodium loading (1.0, 2.0 and 3.0 wt. % Rh) at different temperatures (20, 25, 30 and 35 °C) and constant AB concentration (200 mM, 64 mg). The results reveal no trend in activation energy for the nucleation step while a decrease in activation energy for the autocatalytic surface growth step is noticeable. Additionally, activation energies for the methanolysis of AB catalyzed by Rh(0)/nanoCeO₂ decreases from 75.0 ± 2.0 to 64.6 ± 2.0 kJ·mol⁻¹ with an increasing rhodium

loading from 1.0 to 3.0 wt. % Rh indicating the effect of rhodium loading on the activation energy and kinetics of the reaction. The kinetic studies reveal that methanolysis is first order with respect to catalyst concentration and zero order with regard to substrate concentration. Leaching test clearly demonstrates that rhodium(0) nanoparticles are the true heterogeneous catalyst in hydrogen generation from the methanolysis of AB. High activity and stability of the nanoceria supported rhodium(0) nanoparticles can be attributed to the unique nature of ceria support. In the reducible oxide, Ce³⁺ defects can be formed under the conditions of catalytic reaction. Thus, an excess negative charge on the oxide surface is built up, which can bind the rhodium(0) nanoparticles strongly. This favorable interaction between the ceria support and metal nanoparticles makes the rhodium(0) nanoparticles strongly binding the surface of support.

The facile preparation and high catalytic activity of the nanoceria supported rhodium(0) nanoparticles make them attractive catalysts in hydrogen generation from solid hydrogen storage materials such as ammonia borane which can be used for hydrogen supply in fuel cell applications.

Acknowledgements

Partial support by Turkish Academy of Sciences and TUBITAK for a scholarship to DÖ is gratefully acknowledged. We thank to Dr. Önder Metin for STEM-EDS analysis.

References

- [1] A. Staubitz, A.P.M. Robertson, I. Manners, Chem. Rev. 110 (2010) 4079–4124.
- [2] M. Yadav, Q. Xu, Energy Environ. Sci. 5 (2012) 9698–9725.
- [3] J.E. Mason, Energy Policy 35 (2007) 1315–1329.
- [4] J.O.M. Bockris, Int. J. Hydrogen Energy 27 (2002) 731–740.
- [5] P.V. Ramachandran, P.D. Gagare, Inorg. Chem. 46 (2007) 7810–7817.
- [6] W.W. Zhan, Q.L. Zhu, Q. Xu, ACS Catal. 6 (2016) 6892–6905.
- [7] Y.C. Hu, Y.Z. Wang, R. Su, C.R. Cao, F. Li, C.W. Sun, Y. Yang, P.F. Guan, D.W. Ding, Z.L. Wang, W.H. Wang, Adv. Mater. 28 (2016) 10293–10297.
- [8] S.B. Kalidindi, U. Sanyal, B.R. Jagirdar, Phys. Chem. Chem. Phys. 10 (2008) 5870–5874.
- [9] Q. Yao, M. Huang, Z. Lu, Y. Yang, Y. Zhang, X. Chen, Z. Yang, Dalton Trans. 44 (2015) 1070–1076.
- [10] M. Yurderi, A. Bulut, I.E. Ertas, M. Zahmakiran, M. Kaya, Appl. Catal. B: Environ. 165 (2015) 169–175.
- [11] P. Li, Z. Xiao, Z. Liu, J. Huang, Q. Li, D. Sun, Nanotechnology 26 (2015) 025401.
- [12] C. Yu, J. Fu, M. Muzzio, T. Shen, D. Su, J. Zhu, S. Sun, Chem. Mater. 29 (2017) 1413–1418.
- [13] D. Özhava, N.Z. Kılıçaslan, S. Özkar, Appl. Catal. B: Environ. 162 (2015) 573–582.
- [14] S.B. Kalidindi, A.A. Vermekar, B.R. Jagirdar, Phys. Chem. Chem. Phys. 11 (2009) 770–775.
- [15] D. Sun, V. Mazumder, O. Metin, S. Sun, ACS Catal. 2 (2012) 1290–1295.
- [16] H. Erdogan, Ö. Metin, S. Özkar, Phys. Chem. Chem. Phys. 11 (2009) 10519–10525.
- [17] X. Yang, J.K. Sun, M. Kitta, H. Pang, Q. Xu, Nat. Catal. 1 (2018) 214–220.
- [18] D. Sun, P. Li, B. Yang, Y. Xu, J. Huang, Q. Li, RSC Adv. 6 (2016) 105940–105947.
- [19] H. Erdogan, Ö. Metin, S. Özkar, Catal. Today 170 (2011) 93–98.
- [20] H.B. Dai, X.D. Kang, P. Wang, Int. J. Hydrogen Energy 35 (2010) 10317–10323.
- [21] S. Peng, J. Liu, J. Zhang, F. Wang, Int. J. Hydrogen Energy 40 (2015) 10856–10866.
- [22] S. Çalışkan, M. Zahmakiran, S. Özkar, Appl. Catal. B: Environ. 93 (2010) 387–394.
- [23] J.K. Sun, W.W. Zhan, T. Akita, Q. Xu, J. Am. Chem. Soc. 137 (2015) 7063–7066.
- [24] Q.-L. Zhu, Q. Xu, Chem. 1 (2016) 220–245.
- [25] Q. Yao, Z.-H. Lu, W. Huang, X. Chen, J. Zhu, J. Mater. Chem. A 4 (2016) 8579–8583.
- [26] Q. Yao, W. Shi, G. Feng, Z.-H. Lu, X. Zhang, D. Tao, D. Kong, X. Chen, J. Power Sources 257 (2014) 293–299.
- [27] D. Özhava, S. Özkar, Int. J. Hydrogen Energy 40 (2015) 10491–10501.
- [28] D. Özhava, S. Özkar, Appl. Catal. B: Environ. 181 (2016) 716–726.
- [29] D. Özhava, S. Özkar, Mol. Catal. 439 (2017) 50–59.
- [30] Q. Dai, S. Bai, X. Wang, G. Lu, Appl. Catal. B: Environ. 129 (2013) 580–588.
- [31] S. Chunwen, L. Hong, W.Z. Xiang, C. Liquan, H. Xuejie, Chem. Lett. 33 (2004) 662–663.
- [32] A.J. Bard, R. Parsons, J. Jordan, Standard Potentials in Aqueous Solution, Marcel Dekker Inc., New York, 1985.
- [33] M. Cargnello, V. Doan-Nguyen, T. Gordon, R. Diaz, E. Stach, R. Gorte, P. Fornasiero, C. Murray, Science 341 (2013) 771–773.
- [34] C. Sun, H. Li, L. Chen, Energy Environ. Sci. 5 (2012) 8475–8505.
- [35] Z. Zhang, Z.-H. Lu, H. Tan, X. Chen, Q. Yao, J. Mater. Chem. A 3 (2015) 23520–23529.
- [36] S. Hosokawa, Y. Fujinami, H. Kanai, J. Mol. Catal. A: Chem. 240 (2005) 49–54.
- [37] C. Sun, H. Li, L. Chen, J. Phys. Chem. Solids 68 (2007) 1785–1790.

- [38] C. Sun, L. Chen, Eur. J. Inorg. Chem. 26 (2009) 3883–3887.
- [39] R.S. Suppino, R. Landers, A.J.G. Cobo, Appl. Catal. A 452 (2013) 9–16.
- [40] S. Hosokawa, S. Nogawa, M. Taniguchi, K. Utani, H. Kanai, S. Imamura, Appl. Catal. A 288 (2005) 67–73.
- [41] S. Hosokawa, H. Kanai, K. Utani, Y. Taniguchi, Y. Saito, S. Imamura, Appl. Catal. B Environ. 45 (2003) 181–187.
- [42] S. Akbayrak, Y. Tonbul, S. Özkar, Appl. Catal. B. Environ. 198 (2016) 162–170.
- [43] S. Akbayrak, O. Taneroğlu, S. Özkar, New J Chem. 41 (2017) 6546–6552.
- [44] Y. Tonbul, S. Akbayrak, S. Özkar, Int. J. Hydrogen Energy 41 (2016) 11154–11162.
- [45] S. Akbayrak, Y. Tonbul, S. Özkar, Dalton Trans. 45 (2016) 10969–10978.
- [46] S. Akbayrak, Y. Tonbul, S. Özkar, Appl. Catal. B: Environ. 206 (2017) 384–392.
- [47] C. Sun, J. Sun, G. Xiao, H. Zhang, X. Qiu, H. Li, L. Chen, J. Phys. Chem. B 110 (2006) 13445–13452.
- [48] K. Sevcikova, L. Szabova, M. Kettner, P. Homola, N. Tsud, S. Fabris, V. Matolin, V. Nehasil, J. Phys. Chem. C 120 (2016) 5468–5476.
- [49] E.A. Derevyannikova, T. Yu, L.S. Kardash, E.M. Kibis, V.A. Slavinskaya, O.A. Svetlichnyi, A.S. Stonkus, A.I. Ivanova, Boronin Phys. Chem. Chem. Phys. 19 (2017) 31883–31897.
- [50] M.A. Watzky, R.G. Finke, J. Am. Chem. Soc. 119 (1997) 10382–10400.
- [51] J.A. Widegren, J.D. Aiken, S. Özkar, R.G. Finke, Chem. Mater. 13 (2001) 312–324.
- [52] V. Mevellec, A. Nowicki, A. Roucoux, C. Dujardin, P. Granger, E. Payen, K. Philippot, New J. Chem. 30 (2006) 1214–1219.
- [53] Z.W. Sieh, R. Gronsky, A.T. Bell, J. Catal. 170 (1997) 62–74.
- [54] Z.W. Sieh, R. Gronsky, A.T. Bell, J. Catal. 170 (1997) 62–74.
- [55] Q. Yao, Z.-H. Lu, Y. Jia, X. Chen, X. Liu, Int. J. Hydrogen Energy 40 (2015) 2207–2215.
- [56] S.S. Lee, W. Song, M. Cho, H.L. Puppala, P. Nguyen, H. Zhu, L. Segatori, V.L. Colvin, ACS Nano 7 (2013) 9693–9703.